RSC Advances

PAPER

View Article Online
View Journal | View Issue

Cite this: *RSC Adv.*, 2017, **7**, 21085

Spectroscopic characterization of $SrB_4O_7:Tm^{2+}$, a potential laser material and optical temperature sensor

Piotr Solarz, *[a] Jarosław Komar, [a] Michał Głowacki,[b] Marek Berkowski[b] and Witold Ryba-Romanowski [a]

Received 30th January 2017
Accepted 2nd April 2017

DOI: 10.1039/c7ra01282a

rsc.li/rsc-advances

Polycrystalline samples of SrB_4O_7:1% Tm^{2+} were prepared in air by a solid state reaction method. High resolution spectra and decay curves for infrared luminescence related to the intraconfigurational $^2F_{5/2} \rightarrow {}^2F_{7/2}$ transition and for visible luminescence related to the interconfigurational transition between the lowest energy state of the $4f^{12}5d$ configuration and the ground $^2F_{7/2}$ state of the $4f^{13}$ configuration of Tm^{2+} were recorded as a function of temperature between 5 and 350 K. Energies of crystal field levels of the $^2F_{5/2}$ and $^2F_{7/2}$ multiplets and the $^2F_{5/2}$ lifetime value were determined from low temperature measurements. With these data room temperature emission and absorption spectra were calibrated in the cross-section units. It was found that the infrared emission in $SrB_4O_7:Tm^{2+}$ is long-lived with a lifetime value of 9.5 ms and its spectrum indicates that stimulated emission near 1.18 nm may be feasible. Examination of recorded decay curves for the visible luminescence revealed that the lifetime of the lowest energy state of the $4f^{12}5d$ configuration depends weakly on temperature in the region 5–280 K and then shows a steep decrease when the temperature grows from about 290 K to 350 K. The evaluated values of the thermal sensitivity parameter S for $SrB_4O_7:Tm^{2+}$ in the region 300–330 K (27–57 °C) exceed 3.9% per K with a peak at 320 K (47 °C) equal to 6.30% per K. The S value is the highest reported thus far for luminescence thermometers operating in physiological temperatures.

1 Introduction

There is a long lasting interest in rare earth-doped crystals and glasses. In the past attention has been directed mainly toward finding new laser crystals and designing laser devices. In an enormous number of published papers, laser operation for Nd^{3+}, Ho^{3+}, Er^{3+}, Tm^{3+} and Yb^{3+} in a variety of host crystals has been reported and solid state lasers employing some of these systems are now commercially available. Physicochemical and laser properties of these materials have been reported in several review works, *e.g.* in an exhaustive review by Kaminskii.[1] The search for new laser active crystals is continuing and is directed mainly toward finding better and cheaper laser hosts.[2–4] Crystals doped with divalent rare earth ions have been studied, too. Interest in these systems resulted from an expectation that owing to low energies of the $4f^N{}^{-1}5d$ excited configurations the broad and intense absorption bands related to parity allowed inter-configurational transitions in divalent rare earth ions would be beneficial for optical pumping. This expectation has not been corroborated, however. In early works the alkaline fluoride host crystals have been chosen and laser operation has been demonstrated in $CaF_2:Sm^{2+}$,[5,6] $SrF_2:Sm^{2+}$,[7,8] $CaF_2:Dy^{2+}$ (ref. 9–11) and $CaF_2:Tm^{2+}$,[12,13] but only at cryogenic temperatures. Attempts to achieve room temperature laser operation in crystals doped with Sm^{2+} or Dy^{2+} were unsuccessful because their luminescence bandwidths were found to grow adversely with increasing temperature. Room temperature laser operation in $CaF_2:Tm^{2+}$ could not be achieved as a consequence of an adverse ground state absorption of Tm^{3+} ions (about 80% of thulium ions in CaF_2 host was present in the trivalent state).

Recently, a considerable interest has been directed to optical temperature sensing that offers a possibility to measure the temperature remotely. Numerous papers published during last decade have been devoted to elaborate various methods of temperature sensing and potential sensors that may be employed for this purpose. A variety of thermometers for thermal sensing based on organic fluorophores, quantum dots, bio-molecules and rare earth-doped systems have been described and their sensing capabilities compared. Achievements and current knowledge in this field are presented in valuable review works published recently *e.g.*[14–17] Phosphor thermometers based on luminescent rare earth ions in inorganic hosts are especially attractive because they offer rich energy level structures and are able to show luminescence transitions in a vast spectral region

[a]*Institute of Low Temperature and Structure Research, Polish Academy of Sciences, ul. Okólna 2, 50-422 Wrocław, Poland. E-mail: solarz@int.pan.wroc.pl; Fax: +48-713441029; Tel: +48-713435021*

[b]*Institute of Physics, Polish Academy of Sciences, al. Lotników 32/46, 02-668 Warsaw, Poland*

from UV to near infrared. Phosphor thermometers investigated thus far contained trivalent luminescent rare earth ions Nd^{3+}, Eu, Dy, Ho, Er, Tm.

In the present paper we deal with spectroscopic features of divalent thulium ions in SrB_4O_7 host. Currently, the interest in oxide crystals doped with divalent rare earth ions is stimulated by the search for efficient phosphors able to convert the radiation of blue light emitting diodes (LED) into white light, providing thereby new sources for lighting purposes. The discovery of intense luminescence in SrB_4O_7 host doped with Eu^{2+} (ref. 18) and with Sm^{2+} ions[19] has proved that oxide host crystals are worth considering. In fact, numerous visible phosphors based on Eu^{2+}-doped hosts have been recently fabricated and characterized, *e.g.*: Ca_2SiO_4:Eu^{2+},[20] $CaSrSiO_4$:Eu^{2+},[21] $Ba_3Si_6O_{12}N_2$:Eu^{2+} (ref. 22) and many sulphides.[23]

Considerable less attention has been paid to Sm^{2+}-doped systems. Nevertheless recent papers dealing with the SrB_4O_7:Sm^{2+} phosphor have demonstrated its suitability for application as optical pressure sensors at high temperatures.[24–26] Peculiarities of emission spectra related to the intra-configurational transitions of Sm^{2+} in SrB_4O_7:Sm^{2+} have been reported in ref. 27–29. Effect of temperature on intensities of inter- and intra-configurational transitions and on luminescence lifetime of SrB_4O_7:Sm^{2+} have been studied in ref. 30 and 31. Just recently it has been demonstrated that SrB_4O_7:5% Sm^{2+} system is promising for application as an optical sensor characterized by a high relative decay time temperature sensitivity in a wide temperature region with a record value of 3.36% per K at 550 K.[32]

The search for phosphors based on divalent thulium ions is hampered by the fact that these ions are less stable than Eu^{2+} and Sm^{2+} ions. As far as we know only two papers published in the past provide fundamental information on luminescence of Tm^{2+} ions in oxide crystals. The paper by Schipper *et al.*[33] has reported the first observation of the $4f^{12}5d \rightarrow 4f^{13}$ emission of Tm^{2+} in SrB_4O_7 powder samples prepared by a solid state reaction in a reducing atmosphere consisting of 25% H_2 and 75% N_2. Authors have analysed and interpreted emission and excitation spectra recorded at 4.2 K and proposed mechanisms governing the excited state relaxation dynamics in the temperature region between 4.2 K and 300 K. In the paper by Peterson *et al.*[34] the room temperature diffuse reflectance spectra of SrB_4O_7:Tm^{2+} powders fired at temperatures ranging from 650 °C to 900 °C in air or in Ar/H_2 atmosphere have been recorded and analysed. Authors have shown that the reduction from Tm^{3+} to Tm^{2+} in SrB_4O_7 occurred also for samples fired in air though a significant fraction of incorporated thulium ions still was present in the trivalent state.[34] The outstanding feature of the SrB_4O_7:RE^{2+} (RE = Eu, Sm, Tm) stems from the stability of oxidation state of incorporated rare earth ions combined with a large transparency region of the host crystal stretching from UV to about 3000 nm.[35]

Intention of the present work is to determine spectroscopic properties of the SrB_4O_7:Tm^{2+} system that are relevant to its potential for practical application. First, spectral and temporal characteristics of transitions within the $4f^{13}$ configuration of Tm^{2+} are analysed to assess the feasibility of resonantly pumped infrared laser operation near 1.2 μm. Second, the effect of temperature on spectra and decay of visible luminescence related to the inter-configurational $4f^{12}5d \rightarrow 4f^{13}$ transition of Tm^{2+} is investigated aiming at assessment of utility of the SrB_4O_7:Tm^{2+} as an optical temperature sensor.

2 Experimental

Synthesis

SrB_4O_7 polycrystalline samples were prepared by a solid state reaction method. As starting materials $SrCO_3$ (4N5), B_2O_3 (4N), and Tm_2O_3 (5N) were used. Powders were dried for 10 hours and then their appropriate amounts were weighted to obtain following molar composition: $Sr_{0.99}Tm_{0.01}B_4O_7$. Mixed $SrCO_3$ and B_2O_3 were formed into pellets and heated in air for 10 hours in 300 °C and 10 hours in 800 °C. First step of heating is necessary to avoid melting of B_2O_3 before getting in reaction with strontium carbonate. When reaction begins the CO_2 is starting to volatilize and heated pellets begins to swell. Second step of heating causes complete removal of CO_2 from the material. Thoroughly grounded and formed into pellets materials were heated in air again for 24 hours in 800 °C to remove other $SrO–B_2O_3$ phases and obtain pure SrB_4O_7 phase. Then 1% of Tm_2O_3 was added and mixture was heated for the third time for 24 hours in 800 °C. To perform spectroscopic measurement the polycrystalline pellets 17 mm in diameter and 2 mm thick were prepared.

Spectroscopic measurements

High resolution emission spectra were recorded upon ion argon laser excitation 488 nm line with DongWoo Optron setup composed of 750 mm focal length monochromator DM711 (1 cm^{-1} spectral resolution FWHM for 0.02 mm slits), and detection systems: (VIS) PDS-1 with photomultiplier tube R3896 (Hamamatsu) or (IR) PS/TC-1 controller with InGaAs detector model IGA-030-TE2-H Electro-Optical Systems Inc Kinetic measurements were taken employing an experimental set-up consisting of a tunable optical parametric oscillator (OPO) pumped by a third harmonic of a Nd:YAG laser, a double grating monochromator with a 1000 mm focal length, a detection unit incorporating a photomultiplier operating in the visible or a cooled InSb detector operating in near infrared and a Tektronix MDO 4054B-3 Mixed Domain Oscilloscope. The OPO source delivered a train of light pulses with duration of 7 ns and pulse energy of several mJ (depending on wavelength within the 430–600 nm region) with the repetition rate of 20 Hz. The same apparatus was employed to record excitation (PLE) spectra. To perform measurements at low temperature, the samples were installed in a continuous flow liquid helium cryostat equipped with a temperature controller.

Crystallographic structure determination

Phase analysis and structural refinement were performed with a Siemens D5000 diffractometer (Ni-filtered CuKα radiation). Data were collected in the range 20–100° with a step of 0.02° and averaging time of 10 s per step. XRD pattern (Fig. 1) shows pure SrB_4O_7 phase (JCPDS Card No. 15-0801) for undoped sample. In

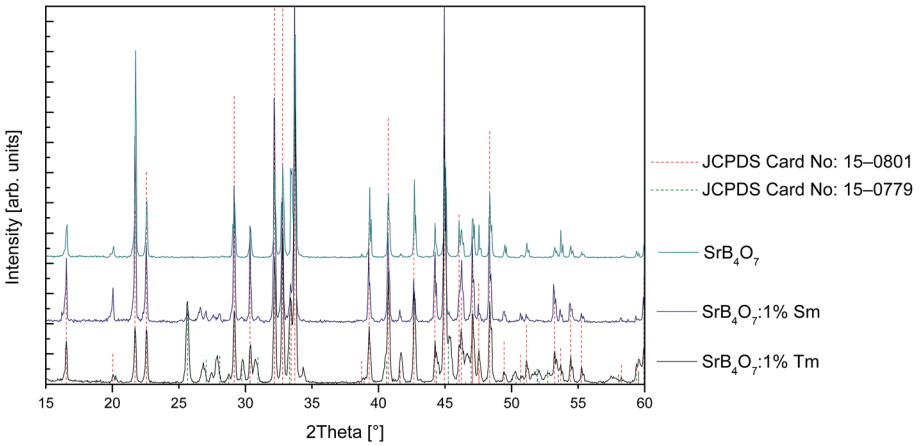

Fig. 1 Diffraction patterns of SrB_4O_7 and SrB_4O_7:1 at% Tm polycrystalline pellets.

thulium doped SrB_4O_7 beside the main tetraborate phase there is a little amount of metaborate (JCPDS Card No. 15-0779) phase visible.

3 Results and discussion

Luminescence of Tm^{2+} ions in crystals may be related to vibronic inter-configurational transitions between the lowest energy state of the $4f^{12}5d$ configuration and the ground $^2F_{7/2}$ state of the $4f^{13}$ configuration and to an intra-configurational $^2F_{5/2} \rightarrow {}^2F_{7/2}$ transition. The spectral region of the latter transition is close to that of the $^2F_{5/2} \rightarrow {}^2F_{7/2}$ transition of isoelectronic Yb^{3+} ions and depends weakly on the host crystal. Resulting luminescence band in CaF_2:Tm^{2+} system has been observed near 1.12 μm and the low temperature laser operation at 1.116 μm has been obtained in the past.[12,13] Peculiarities of the $^2F_{5/2} \rightarrow {}^2F_{7/2}$ luminescence for the SrB_4O_7:Tm^{2+} system have not been determined in previously reported study because weak luminescence lines could not be separated from the background.[33] Also, the room temperature absorption (diffuse reflectance measurement) spectrum recorded for the $^2F_{7/2} \rightarrow {}^2F_{5/2}$ transition in SrB_4O_7:Tm^{2+} did not provide reliable information because of superposed absorption of residual Tm^{3+} ions.[34] It will be shown in the following paragraph that spectra and decay curves recorded in a wide temperature region are able to provide new information on the $^2F_{5/2} \rightarrow {}^2F_{7/2}$ infrared luminescence in SrB_4O_7:Tm^{2+}.

3.1 Effect of temperature on the intra-configurational $^2F_{5/2} \rightarrow {}^2F_{7/2}$ infrared luminescence

Fig. 2 compares luminescence spectra of Tm^{2+} in the near infrared region, recorded at several different temperatures in the region of 5–300 K.

The site symmetry for Tm^{2+} ions in this host is lower than cubic, therefore four crystal field components for the ground $^2F_{7/2}$ multiplet and three crystal field components for the $^2F_{5/2}$ excited multiplet are predicted. Since the population of the crystal field components is governed by the Boltzmann statistics the luminescence spectra are expected to be temperature dependent. It can be seen in Fig. 2 that at 5 K the luminescence spectrum consists of four well separated lines located at 1131.6 nm (8837 cm^{-1}), 1141.3 nm (8762 cm^{-1}), 1152.95 nm (8673 cm^{-1}) and 1180 nm (8475 cm^{-1}). We assign these lines to

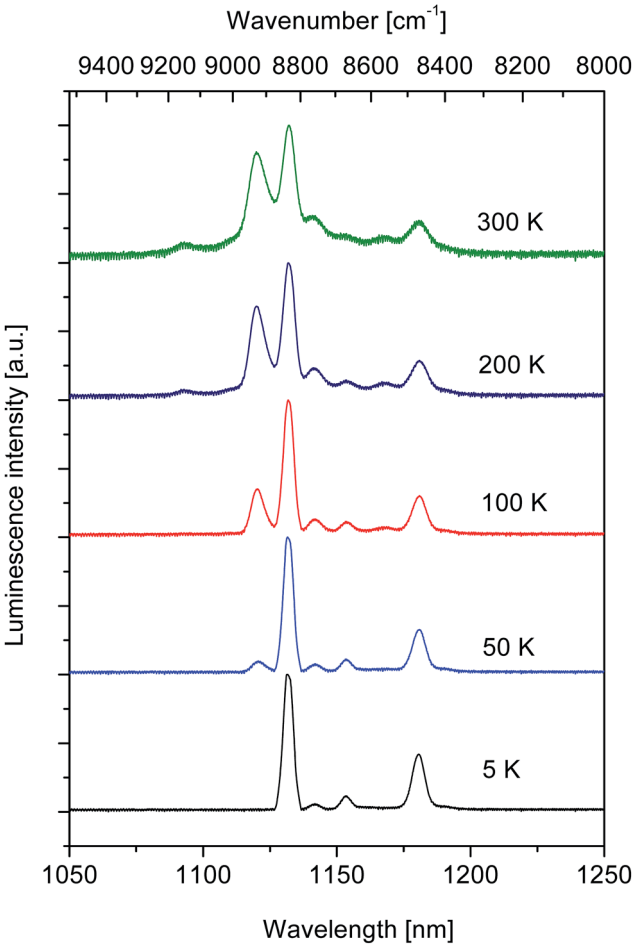

Fig. 2 The $^2F_{5/2} \rightarrow {}^2F_{7/2}$ luminescence spectra of Tm^{2+} ions in SrB_4O_7 host recorded at several different temperatures upon excitation at 488 nm.

transitions from the lowest crystal field component of the $^2F_{5/2}$ excited multiplet to four crystal field components of the ground state. Accordingly, the line located at 1131.6 nm is related to the transition ending on the lowest crystal field component of the ground multiplet (0–0 line) and remaining lines are related to transitions ending on the higher crystal field components located at 75, 164 and 362 cm^{-1}. In the spectrum of the 50 K luminescence an additional line related to transition from the second higher energy component of the initial $^2F_{5/2}$ multiplet appears at 1120.25 nm (8927 cm^{-1}). Above 200 K a weak line peaking at 1093.3 nm (9147 cm^{-1}) contributes to the spectrum. Assuming that it is related to transitions from the highest energy component of the initial state we locate components of the $^2F_{5/2}$ excited multiplet at 8837, 8927 and 9147 cm^{-1}. At higher temperatures the transitions from all crystal field levels of the $^2F_{5/2}$ multiplet contribute to luminescence band and recorded spectra do not show significant differences.

The $^2F_{5/2} \rightarrow {}^2F_{7/2}$ infrared luminescence of Tm^{2+} in SrB_4O_7 is found to be long-lived. Decay curves of this luminescence were recorded at different temperatures in the 5–450 K region. All of them were consistent with a single exponential time dependence providing thereby a set of reliable lifetime values. A plot of measured luminescence lifetimes *versus* temperature is shown in Fig. 3.

Observed increase of the lifetime with growing temperature is due likely to a lengthening effect of self-absorption, commonly encountered during investigation of the $^2F_{5/2} \rightarrow {}^2F_{7/2}$ emission in crystals doped with Yb^{3+}. Therefore we consider the value of 9.5 ms determined from a decay curve recorded at 5 K to be actual $^2F_{5/2}$ lifetime.

In principle the relaxation of the $^2F_{5/2}$ metastable level of Tm^{2+} in SrB_4O_7 is governed by radiative transitions and nonradiative multiphonon transitions. The rate of multiphonon relaxation is expected to be low since a simultaneous emission of six phonons with the highest energy of about 1400 cm^{-1} that are available in the host would be needed to bridge the energy difference of about 8400 cm^{-1} between the $^2F_{5/2}$ and $^2F_{7/2}$ levels. Having this in mind we assume that the measured luminescence lifetime of 9.5 ms is close to the $^2F_{5/2}$ radiative lifetime and we calibrate the $^2F_{5/2} \rightarrow {}^2F_{7/2}$ emission band in units of emission cross-section $\sigma_{em}(\lambda)$ employing the Füchtbauer–Ladenburg relation:

$$\sigma_{em}(\lambda) = \frac{\beta\lambda^5 I(\lambda)}{8\pi c n^2 \tau_{rad} \int \lambda I(\lambda) d\lambda} \quad (1)$$

where β is the luminescence branching ratio (equal to 1 for this transition), $I(\lambda)$ is the emission spectrum intensity, τ_{rad} is the radiative lifetime of the $^2F_{5/2}$ level and n denotes the index of refraction of the crystal. Solid line in Fig. 4 represents the resulting $\sigma_{em}(\lambda)$ spectrum for the experimental $^2F_{5/2} \rightarrow {}^2F_{7/2}$ infrared luminescence band recorded at 300 K. The peak value for the emission cross section of 3.5×10^{-20} cm^2 is advantageously high. However, the terminal level of this transition is the ground state and an actual ability of the system for light amplification will be markedly smaller due to an adverse effect of self-absorption. To assess quantitatively this shortcoming we calculate the spectrum for the $^2F_{7/2} \rightarrow {}^2F_{5/2}$ absorption cross-section employing a so called reciprocity relation. The method is based on the relation between absorption cross-section $\sigma_{abs}(\lambda)$ and emission cross-section $\sigma_{em}(\lambda)$:

$$\sigma_{em}(\lambda) = \frac{Z_{low}}{Z_{up}} \sigma_{abs}(\lambda) \exp\left(\frac{E_{zl} - E(\lambda)}{k_B T}\right) \quad (2)$$

where Z_{low}, Z_{up} are the partition functions for the lower and upper levels, respectively, defined as:

$$Z_{low} = \sum_{i=1}^{n} g_i \exp\left(-\frac{E_i}{k_B T}\right); \; Z_{up} = \sum_{i=1}^{n} g_j \exp\left(-\frac{E_j - E(\lambda)}{k_B T}\right) \quad (3)$$

where g_i and (g_j) are the degeneration of a crystal field level having the E_i and (E_j) energy, respectively. E_{zl} is energy difference between lowest crystal field components of the upper and lower multiplets and k_B is the Boltzmann constant. Inserting

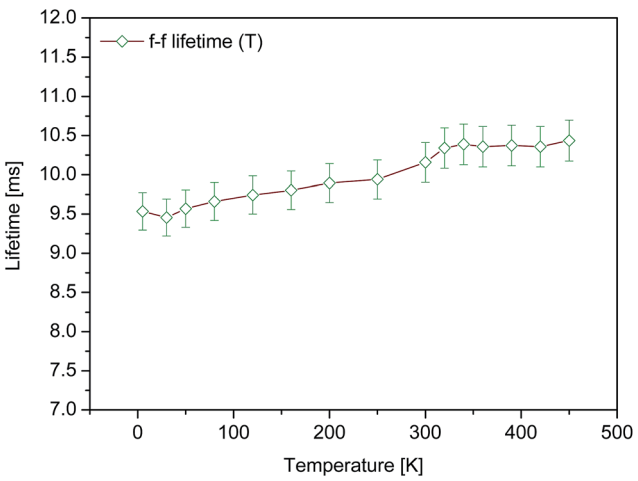

Fig. 3 Lifetime of the $^2F_{5/2}$ multiplet of Tm^{2+} in SrB_4O_7 host plotted *versus* temperature.

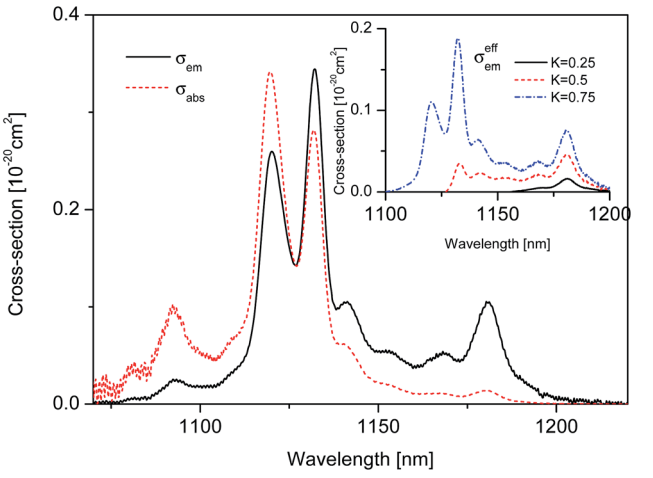

Fig. 4 Room temperature $^2F_{5/2} \rightarrow {}^2F_{7/2}$ luminescence spectrum σ_{em} (solid line) and derived $^2F_{7/2} \rightarrow {}^2F_{5/2}$ absorption spectrum σ_{abs} (dashed line) calibrated in cross-section units for the SrB_4O_7:Tm^{2+} system. Inset shows an effective emission cross-section spectrum $\sigma_{em}^{eff}(\lambda)$ calculated according to eqn (4).

values for energies of crystal field levels determined above to eqn (2) and (3) we obtain the spectrum for the absorption cross section σ_{abs} represented by a dashed line in Fig. 4.

It can be seen that the curve of emission cross-section dominates significantly that of absorption cross-section in the spectral region between 1150 and 1230 nm pointing thereby at positive values of optical amplification coefficient. To predict the wavelength of a potential laser operation the effective emission cross-section function $\sigma_{em}^{eff}(\lambda)$ was evaluated according to the relation:

$$\sigma_{em}^{eff}(\lambda) = K\sigma_{em}(\lambda) - (1 - K)\sigma_{abs}(\lambda) \quad (4)$$

where K is the population inversion parameter defined as the density of excited Tm^{2+} ions divided by the overall density of Tm^{2+} ions in the crystal host. Resulting $\sigma_{em}^{eff}(\lambda)$ spectra calculated for several reasonable values of K are shown in the inset to Fig. 4. It follows from these spectra that the laser operation in SrB_4O_7:Tm^{2+} at 1180 nm can be feasible for low K values. It is worth noticing here that an excited state absorption (ESA) due to allowed transitions from the metastable level to states of the $4f^{N-1}5d$ configuration (ESA), detrimental for stimulated emission in SrF_2:Sm^{2+},[36] cannot affect the emission around 1180 nm in SrB_4O_7:Tm^{2+} because of a large $^2F_{5/2}$–$4f^{N-1}5d$ energy gap.

3.2 Effect of temperature on the $4f^{12}5d \rightarrow 4f^{13}$ visible luminescence

In contrast to the $^2F_{5/2}$ level of the $4f^{13}$ configuration considered above, the lowest energy state of the $4f^{12}5d$ configuration of Tm^{2+} ions depends strongly on the host. Based on careful analysis of low temperature luminescence spectrum it has been located at 17 210 cm^{-1} SrB_4O_7:Tm^{2+} system,[33] that is markedly higher than about 14 000 cm^{-1} found in the past for CaF_2:Tm^{2+} system.[12,13] Due to larger energy gap between the bottom of the $4f^{12}5d$ configuration and the next lower energy $^2F_{5/2}$ state the nonradiative relaxation is suppressed in SrB_4O_7:Tm^{2+} system and an efficient visible emission related to the $4f^{12}5d \rightarrow 4f^{13}$ ($^2F_{7/2}$) transition is observed.

Fig. 5 shows spectra of visible luminescence in the SrB_4O_7:Tm^{2+} system recorded at several sample temperatures in the 300–5 K temperature region. At 300 K the spectrum has a maximum at 595.4 nm and consists of a single broad and smooth band, typical for vibronic transitions. Decrease of temperature down to 110 K affects little the shape of the luminescence band but it brings about a monotonic shift of the band maximum to about 601.2 nm.

During further decrease of temperature the position of maximum is arrested but the intensity of a structure on the short wavelength side of the band, hardly visible at 110 K, grows steadily and eventually at 5 K a group of narrow lines contributes to the spectrum. Details of the 5 K luminescence spectrum shown in Fig. 5 are consistent with those recorded at 4.2 K and reported in the work by Schipper *et al.*[33] proving thereby that we are dealing with the same material. According to the assignment proposed in[33] the structure that appears in the low temperature spectrum of the $4f^{12}5d \rightarrow 4f^{13}$ transition of Tm^{2+} in SrB_4O_7 consists of zero phonon lines and related

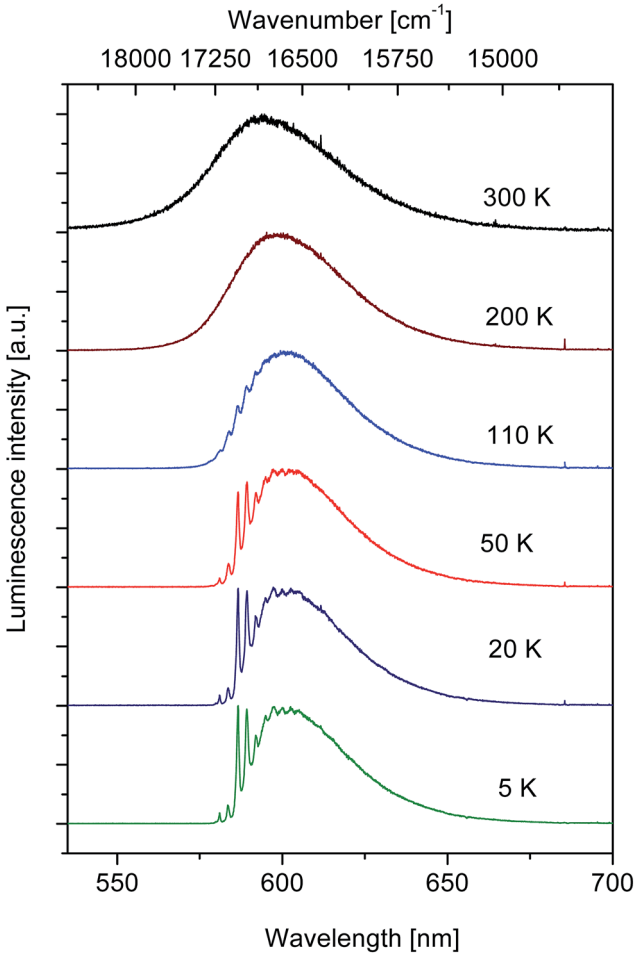

Fig. 5 Effect of temperature on spectral characteristics of visible luminescence in SrB_4O_7:Tm^{2+} system. Excitation wavelength was 488 nm.

progressions. Measurement of the excited state relaxation dynamics was performed when changing the sample temperature in a vast region 5–360 K. It was found that the decay curves of luminescence follow a single exponential time dependence for all temperature points considered. Fig. 6 shows a plot of evaluated time constants (luminescence lifetime values) *versus* sample temperature.

It can be seen that initially the lifetime values decrease gently with increasing temperature and then at about 290 K a very steep decrease occurs. Eventually at 360 K the lifetime value of 5 us was measured. Observed change of lifetime induced by variation of the temperature points at the potential of the system under study for optical thermometry. Commonly, the quality of optical sensors based on temperature-dependent luminescence lifetime is assessed employing a thermal sensitivity parameter S defined by the relation:[32]

$$S = \left|\frac{1}{\tau}\frac{d\tau}{dT}\right| \quad (5)$$

where τ denotes the lifetime value and T denotes the temperature.

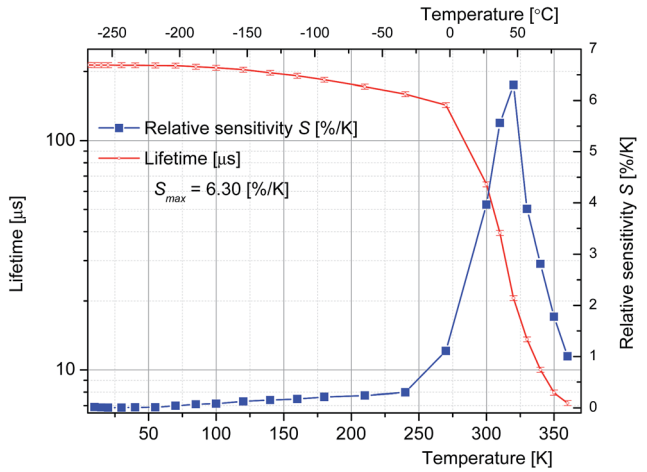

Fig. 6 Lifetime of the $4f^{12}5d \rightarrow 4f^{13}$ ($^2F_{7/2}$) visible emission (red open circles) and calculated thermal sensitivity parameter S (full blue squares) plotted *versus* temperature for the SrB_4O_7:Tm^{2+} system. Lines are only guides for eyes.

The sensitivity parameter was calculated according to eqn (5) above and plotted *versus* temperature in Fig. 6.

The evaluated values of thermal sensitivity parameter S for the SrB_4O_7:Tm^{2+} system in the 300–330 K (27–57 °C) region exceed 3.9% per K with a peak value of 6.30% per K at 320 K (47 °C). It can be seen that in the temperature region between 10 °C and 47 °C the luminescence lifetime values are advantageously high and the S parameter depends linearly on the temperature.

In addition, the SrB_4O_7:Tm^{2+} system shows a broad and intense absorption band stretching from 450 nm to 550 nm favouring thereby an efficient excitation. Moreover, the PLE spectra recorded at 15 °C, 25 °C and 40 °C and compared in Fig. 7 indicate that the excitation efficiency is weakly affected by the temperature in this region. It is worth mentioning that in contrast to crystals doped with trivalent rare earth ions the ion–ion energy transfer processes do not affect significantly spectra and excited state relaxation dynamics of Tm^{2+} ions in SrB_4O_7.

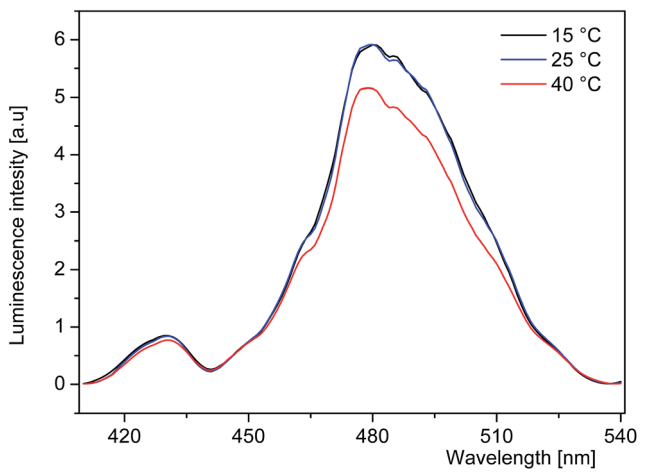

Fig. 7 Excitation spectra of emission at 600 nm recorded at 15, 25, and 40 °C.

Indeed, low temperature luminescence spectra and lifetime of inter-configurational transition reported for SrB_4O_7:0.5% Tm^{2+} in ref. 33 do not differ from those presented above for SrB_4O_7:1% Tm^{2+}. All these features indicate that the SrB_4O_7:-Tm^{2+} system may be a promising optical sensor operating in the physiological temperature region.

Ability to measure temperature changes in living cells is of paramount importance for the detection of pathological states *e.g.* of tumour deceases. Therefore numerous papers published during last decade have been devoted to elaborate various methods of temperature sensing and potential sensors that may be employed for this purpose. In an excellent review paper published recently by Tingting Bai and Ning Gu[17], presenting the state of the art in this topic, thermometers for thermal sensing and imaging of living cells and biological tissues based on organic fluorophores, quantum dots, bio-molecules and rare earth-doped systems are described and their sensing capabilities compared. Reported values of thermal sensitivity parameter S refer to various spans of temperature within the 10–60 °C region. Among non-contact luminescent thermometers the highest values of S parameters have been found for organic fluorophores, *e.g.*: 3.9% per K in the temperature range 32–37 °C for ns decay of "ER thermo yellow" compound[37] and for rare earth metal complexes, *e.g.*: 2.74% per K in the temperature range 25–50 °C for Eu-TTA.[38] Evaluated thermal sensitivity parameters for inorganic rare earth-doped thermometers are markedly lower, however[39–42] with the highest S parameter value of 1.6% per K in the temperature range 10–36 °C reported for $NaYF_4$:Er^{3+},Yb^{3+}.[43] Recently, using a Cr^{3+} to Nd^{3+} emission intensity ratio, the highest 3.48% per K sensitivity has been obtained in the physiological temperature range.[44] The evaluated values of thermal sensitivity parameter S for the SrB_4O_7:-Tm^{2+} system in the 300–330 K (27–57 °C) region exceed 3.9% per K with a peak value of 6.30% per K at 320 K (47 °C), and to our knowledge they are higher than those reported thus far for other luminescent thermometers operating in this temperature region.

4 Conclusions

Based on analysis of the effect of temperature on luminescence spectrum related to the $^2F_{5/2} \rightarrow {}^2F_{7/2}$ intra-configurational transition of Tm^{2+} three crystal field levels of the $^2F_{5/2}$ initial multiplet were located at 8837, 8927 and 9147 cm^{-1} and four crystal field levels of the ground $^2F_{7/2}$ multiplet were located at 75, 164 and 362 cm^{-1} for the SrB_4O_7:Tm^{2+} system. Observed luminescence is long-lived with a lifetime value of 9.5 ms at 5 K. Comparison of the room temperature $^2F_{5/2} \rightarrow {}^2F_{7/2}$ luminescence band calibrated in the cross-section units according to the Füchtbauer–Ladenburg relation to that of the $^2F_{7/2} \rightarrow {}^2F_{5/2}$ absorption band derived by a reciprocity method points at a positive value of optical amplification coefficient in a spectral region between 1150 and 1230 nm. Adverse effect of self-absorption was considered and its importance was assessed based on the calculated effective cross-section spectrum. It was also concluded that an excited state absorption (ESA) due to allowed transitions from the metastable level to states of the

$4f^{N-1}5d$ configuration (ESA), cannot affect the emission around 1.18 μm in $SrB_4O_7:Tm^{2+}$ because of large $4f^{N-1}5d \rightarrow {}^2F_{5/2}$ energy gap. In $SrB_4O_7:Tm^{2+}$ system the lifetime (τ) of intense visible emission related to vibronic inter-configurational transitions between the lowest energy state of the $4f^{12}5d$ configuration and the ground ${}^2F_{7/2}$ state of the $4f^{13}$ configuration of Tm^{2+} changes abruptly when the temperature (T) varies in the region 280–350 K implying utility of this system for luminescence- based thermometry. The evaluated values of thermal sensitivity parameter S for the $SrB_4O_7:Tm^{2+}$ system in the 300–330 K (27–57 °C) region exceed 3.9% per K with a peak value of 6.30% per K at 320 K (47 °C). Therefore, such a phosphor can be used as temperature sensor in biological region of temperatures.

Author contributions

The manuscript was written through contributions of all authors. All authors have given approval to the final version of the manuscript.

Funding sources

NCN under project DEC-2013/09/D/ST5/03878.

Abbreviations

4N	99.99%
4N5	99.995%
5N	99.999%
ESA	Excited state absorption
Eu-TTA	Europium(III) thenoyltrifluoroacetonate trihydrate
FWHM	Full width at half maximum
IR	Infrared
JCPDS	Joint Committee on Powder Diffraction Standards
LED	Light emitting diode
NCN	National Science Centre
S	Thermal sensitivity parameter
VIS	Visible
XRD	X-ray diffraction

Acknowledgements

The work was funded by the National Science Centre (NCN) on the basis of the decision number DEC-2013/09/D/ST5/03878.

References

1 A. A. Kaminskii, *Laser Photonics Rev.*, 2007, **1**, 93–177.
2 X. Zhang, Y. Zhou, J. Ren, D. Lu, H. Yu, Z. Wang, S. Guo and X. Xu, *CrystEngComm*, 2016, **18**, 5338–5343.
3 L. Zhang, H. Lin, G. Zhang, X. Mateos, J. M. Serres, M. Aguiló, F. Díaz, U. Griebner, V. Petrov, Y. Wang, P. Loiko, E. Vilejshikova, K. Yumashev, Z. Lin and W. Chen, *Opt. Express*, 2017, **25**, 3682–3693.
4 A. Rudenkov, V. Kisel, A. Yasukevich, K. Hovhannesyan, A. Petrosyan and N. Kuleshov, *Opt. Lett.*, 2016, **41**, 5805–5808.
5 P. P. Sorokin and M. J. Stevenson, *IBM J. Res. Dev.*, 1961, **5**, 56–58.
6 W. Kaiser, C. G. B. Garrett and D. L. Wood, *Phys. Rev.*, 1961, **123**, 766–776.
7 P. P. Sorokin, M. J. Stevenson, J. R. Lankard and G. D. Pettit, *Phys. Rev.*, 1962, **127**, 503–508.
8 D. L. Wood and W. Kaiser, *Phys. Rev.*, 1962, **126**, 2079–2088.
9 A. Yariv, *Proc. IRE*, 1962, **50**, 1699.
10 L. F. Johnson, *Proc. IRE*, 1962, **50**, 1691.
11 Z. J. Kiss and R. C. Duncan, *Proc. IRE*, 1962, **50**, 1531.
12 Z. J. Kiss and R. C. Duncan, *Proc. IRE*, 1962, **50**, 1532.
13 R. C. Duncan and Z. J. Kiss, *Appl. Phys. Lett.*, 1963, **3**, 23–24.
14 D. Jaque and F. Vetrone, *Nanoscale*, 2012, **4**, 4301–4326.
15 X. Wang, Q. Liu, Y. Bu, C.-S. Liu, T. Liu and X. Yan, *RSC Adv.*, 2015, **5**, 86219–86236.
16 C. D. S. Brites, P. P. Lima, N. J. O. Silva, A. Millán, V. S. Amaral, F. Palacio and L. D. Carlos, *Nanoscale*, 2012, **4**, 4799–4829.
17 T. Bai and N. Gu, *Small*, 2016, 1–21.
18 A. Meijerink, J. Nuyten and G. Blasse, *J. Lumin.*, 1989, **44**, 19–31.
19 A. Lacam and C. Chateau, *J. Appl. Phys.*, 1989, **66**, 366–372.
20 Y. Y. Luo, D. S. Jo, K. Senthil, S. Tezuka, M. Kakihana, K. Toda, T. Masaki and D. H. Yoon, *J. Solid State Chem.*, 2012, **189**, 68–74.
21 S. Tezuka, Y. Sato, T. Komukai, Y. Takatsuka, H. Kato and M. Kakihana, *Appl. Phys. Express*, 2013, **6**, 72101.
22 C. Yasushita, H. Kato and M. Kakihana, *J. Inf. Disp.*, 2012, **13**, 107–111.
23 P. F. Smet, I. Moreels, Z. Hens and D. Poelman, *Materials*, 2010, **3**, 2834–2883.
24 F. Datchi, A. Dewaele, P. Loubeyre, R. Letoullec, Y. Le Godec and B. Canny, *High Pressure Res.*, 2007, **27**, 447–463.
25 S. V. Rashchenko, A. Y. Likhacheva and T. B. Bekker, *High Pressure Res.*, 2013, **33**, 720–724.
26 Q. Jing, Q. Wu, Y. Liu, Y. Zhang, S. Liu, L. Liu, J. Xu and Y. Bi, *High Pressure Res.*, 2013, **33**, 725–733.
27 H. Liang, Q. Zeng, T. Hu, S. Wang and Q. Su, *Solid State Sci.*, 2003, **5**, 465–467.
28 R. Stefani, A. D. Maia, E. E. S. Teotonio, M. A. F. Monteiro, M. C. F. C. Felinto and H. F. Brito, *J. Solid State Chem.*, 2006, **179**, 1086–1092.
29 J. Sun, J. Zhu, X. Liu and H. Du, *J. Rare Earths*, 2012, **30**, 1084–1087.
30 S. Sakirzanovas, A. Katelnikovas, D. Dutczak, A. Kareiva and T. Jüstel, *J. Lumin.*, 2012, **132**, 141–146.
31 P. Solarz, M. Karbowiak, M. Głowacki, M. Berkowski, R. Diduszko and W. Ryba-Romanowski, *J. Alloys Compd.*, 2016, **661**, 419–427.
32 Z. Cao, X. Wei, L. Zhao, Y. Chen and M. Yin, *ACS Appl. Mater. Interfaces*, 2016, **8**, 34546–34551.
33 W. J. Schipper, A. Meijerink and G. Blasse, *J. Lumin.*, 1994, **62**, 55–59.
34 J. R. Peterson, W. Xu and S. Dai, *Chem. Mater.*, 1995, **7**, 1686–1689.
35 R. C. Ropp, in *Encyclopedia of the Alkaline Earth Compounds*, Elsevier, 2013, pp. 481–635.

36 S. A. Payne, L. L. Chase, W. F. Krupke and L. A. Boatner, *J. Chem. Phys.*, 1988, **88**, 6751–6756.
37 H. Itoh, S. Arai, T. Sudhaharan, S.-C. Lee, Y.-T. Chang, S. Ishiwata, M. Suzuki and E. B. Lane, *Chem. Commun.*, 2016, **52**, 4458–4461.
38 M. Suzuki, V. Tseeb, K. Oyama and S. Ishiwata, *Biophys. J.*, 2007, **92**, L46–L48.
39 F. Vetrone, R. Naccache, A. Zamarrón, A. J. De La Fuente, F. Sanz-Rodríguez, L. M. Maestro, E. M. Rodriguez, D. Jaque, J. G. Sole and J. A. Capobianco, *ACS Nano*, 2010, **4**, 3254–3258.
40 H. Peng, M. I. J. Stich, J. Yu, L. N. Sun, L. H. Fischer and O. S. Wolfbeis, *Adv. Mater.*, 2010, **22**, 716–719.
41 A. Siaï, P. Haro-González, K. Horchani-Naifer and M. Férid, *Sens. Actuators, B*, 2016, **234**, 541–548.
42 G. Jiang, X. Wei, Y. Chen, C. Duan, M. Yin, B. Yang and W. Cao, *Mater. Lett.*, 2015, **143**, 98–100.
43 P. Rodríguez-Sevilla, Y. Zhang, P. Haro-González, F. Sanz-Rodríguez, F. Jaque, J. G. Solé, X. Liu and D. Jaque, *Adv. Mater.*, 2016, **28**, 2421–2426.
44 L. Marciniak, A. Bednarkiewicz, J. Drabik, K. Trejgis and W. Strek, *Phys. Chem. Chem. Phys.*, 2017, **19**, 7343–7351.